Heterogeneous Reactions of Sulfur Dioxide on Typical Mineral Particles

ARTICLE *in* THE JOURNAL OF PHYSICAL CHEMISTRY B · JULY 2006

Impact Factor: 3.3 · DOI: 10.1021/jp0617773 · Source: PubMed

7 AUTHORS, INCLUDING:

Xingying Zhang
National Satellite Meteorological Center
30 PUBLICATIONS **553** CITATIONS
SEE PROFILE

Guoshun Zhuang
Fudan University
111 PUBLICATIONS **4,523** CITATIONS
SEE PROFILE

Jian-Min Chen
Fudan University
166 PUBLICATIONS **2,680** CITATIONS
SEE PROFILE

Peng Zhang
Sichuan University
58 PUBLICATIONS **388** CITATIONS
SEE PROFILE

Heterogeneous Reactions of Sulfur Dioxide on Typical Mineral Particles

Xingying Zhang,[‡,§,†] Guoshun Zhuang,[*,‡,§,⊥,#] Jianmin Chen,[‡] Ying Wang,[§] Xiao Wang,[‡] Zhisheng An,[⊥] and Peng Zhang[||]

Center for Atmospheric Chemistry Study, Department of Environmental Science & Engineering, Fudan University, Shanghai 200433, China, Center for Atmospheric Environmental Study, Department of Chemistry, Beijing Normal University, Beijing 100875, China, State Key Laboratory of Loess & Quaternary Geology, Institute of Earth Environment, CAS, Xian 710075, China, NZC/LAPC, Institute of Atmospheric Physics, Chinese Academy of Science, Beijing 100029, China, and Key Laboratory of Radiometric Calibration and Validation for Environmental Satellites, National Satellite Meteorological Center, China Meteorological Administration (LRCVES/CMA), Beijing 100081, China

Received: March 22, 2006; In Final Form: April 29, 2006

The heterogeneous reaction of SO_2 on Al_2O_3, CaO, TiO_2, MgO, FeOOH, Fe_2O_3, MnO_2, and SiO_2, as well as authentic aerosol sample, was investigated by using a White Cell coupled with *in situ*-FTIR and Diffuse Reflectance Infrared Fourier Transform Spectroscopy (DRIFTS). Simultaneous observations of reactants and products were performed to obtain full information on the mechanism and kinetics of the reactions. SO_2 was irreversibly adsorbed to form surface sulfite (SO_3^{2-}), bisulfite (HSO_3^-), and sulfate (SO_4^{2-}). The reactivity order of these particles is the following: FeOOH > Al_2O_3 > mixture > MgO > Fe_2O_3 > SiO_2. Field-collected aerosol showed significant activity for the oxidation of SO_2. The uptake coefficient of SO_2 on Al_2O_3 with different acidity varied in the order of basic Al_2O_3 > neutral Al_2O_3 > acidic Al_2O_3. The surface-active oxygen and hydroxyl might be the key factors for the conversion of SO_2 to SO_4^{2-}. The faster reaction rate could be achieved with greater surface area on particles with the same mass. On the basis of the same surface area Fe_2O_3 could be most reactive in the reaction with SO_2 compared with all other particles. The apparent rate constants were determined to be 1.35×10^{-2} and 9.4×10^{-3} for uptake on Al_2O_3 and MgO, respectively, which are the same as the results of other scientists.

Introduction

Gas-phase sulfur and nitrogen oxides could react with mineral aerosol to form particulate sulfate and nitrate. Recent atmospheric modeling studies have suggested that mineral aerosols have a significant impact on the chemistry of trace gases in the troposphere, such as SO_2 and NO_x.[1] SO_2 could be oxidized to sulfuric acid and, in turn, to sulfate through several pathways, including in clouds and in the liquid droplets in the troposphere. Atmospheric sulfate particles are known to play a role in the global climate by scattering solar radiation and increasing the number of cloud condensation nuclei (CCN).[2,3] Sulfate-coated mineral dust particles can change this impact as they participate in the hygroscopic deliquescence and efflorescence cycles.[4,5] Sulfate particles are known to affect climate by scattering solar radiation, resulting in a net cooling effect, as well as acting as cloud condensation nuclei (CCN) and thereby indirectly affecting climate.[6] Nearly half of the global emissions of SO_2 are converted to particulate sulfate, and this sulfate is often associated with particles, either sea-salt over the ocean or mineral dust over the continent.[7] Conversion of SO_2 to SO_4^{2-} in sea-salt aerosols might account for up to 60% of the oxidation in the marine troposphere.[8] Mineral aerosols also participate in the accumulation of particulate sulfate in the troposphere. In the spring each year Asian dust, i.e., mineral aerosol, carried other chemical species, such as sulfate and nitrate derived from SO_x and NO_x, and transported them to Eastern China, Korea, Japan, the Pacific Ocean, and even the west coast of the U.S.[9,10] It was reported that Asian dust collected in Korea contained aerosols reacted with NO_x and SO_x, especially when it had passed through an industrialized region of China.[11,12] Asian dusts collected in Japan and Hong Kong were also reported to contain aerosols reacted with NO_x, SO_x, and sea-salts.[13,14] Asian dusts collected in Japan were reported to experience chemical modification during their long-range transport.[15,16]

It is well-known that SO_2 can be oxidized to sulfate in aqueous aerosol by ozone and hydrogen peroxide.[8,17−22] However, the mechanisms of sulfate formation on mineral aerosol are not clearly understood.[8] It has been proposed that ozone could oxidize adsorbed sulfite to sulfate on particle surfaces.[23] S(IV) oxidation by molecular oxygen could be catalyzed by iron-containing species.[18] Recently, the heterogeneous interactions between gaseous molecules with wet or dry aerosol particles have gained considerable interest since they could significantly alter the gas-phase chemistry in the atmosphere. In the late 1960s and 1970s, laboratory studies of the heterogeneous reactions of SO_2 were undertaken with the recognition that gas−solid reactions could be important in the atmosphere.[24−26] It has been noted that the removal of SO_2 from gas mixtures was more efficient in the presence of certain solid materials. Metal oxides have been studied as adsorbents to clean the industrial emissions of SO_2.[27,28] Many works have been done

* Address correspondence to this author. Fax: 8621-65642080. E-mail: gzhuang@bnu.edu.cn.
‡ Fudan University.
§ Beijing Normal University.
|| China Meteorological Administration.
⊥ Institute of Earth Environment, CAS.
Institute of Atmospheric Physics, CAS.
† Current address: Key Laboratory of Radiometric Calibration and Validation for Environmental Satellites, National Satellite Meteorological Center, China Meteorological Administration (LRCVES/CMA).

10.1021/jp0617773 CCC: $33.50
Published on Web 06/08/2006

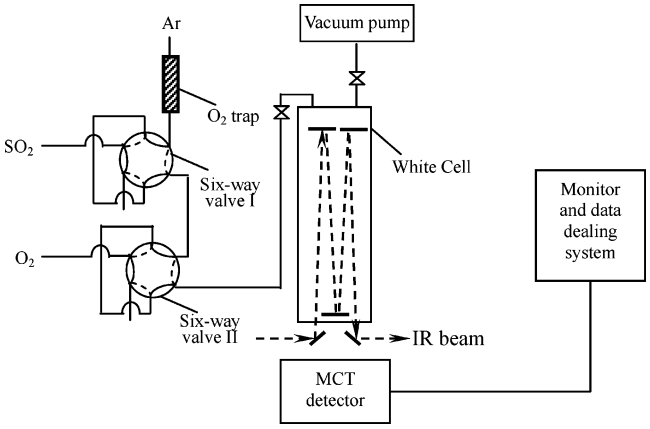

Figure 1. Schematic diagram of the reaction system in the White Cell apparatus.

on aerosol's profound impacts on NO_x,[29, 30] CS_2 ,[31−33] COS,[34, 35] and volatile components.[36] However, the reaction of SO_2 on mineral aerosols is not fully understood, as the mechanism of SO_2 oxidation on the mineral particles to form sulfate is not clear.[37−39] As both the sulfate and mineral aerosol play an important role in the global environmental change,[40−42] a better understanding of the origin and the mechanism of sulfate formation on the mineral aerosols are highly desirable. In this study, the mechanisms of the heterogeneous uptake and oxidation of SO_2 on the typical mineral oxides and the field-collected mineral aerosol at ambient temperature are investigated.

Experimental Section

***In Situ* FTIR Measurement.** For FTIR measurements, approximately 30 mg of oxide sample was prepared by pressing it into a pallet with a diameter of 13 mm and then secured inside the infrared cell (White Cell reactor—the variable path length path cell, Model 19-V, Infrared Analysis, Inc.) through the sample holder jaws made of Teflon. Figure 1 shows a schematic diagram of the reaction system. The details about the White Cell have been given elsewhere.[34,35] The infrared cell is connected to a vacuum chamber through a Teflon tube and a glass gas manifold with ports for gas introduction and a vacuometer. The volume of the system is 1.68 L and the total optical path of the cylindrical borosilicate glass vessel with two KCl windows at the bottom is 19.2 m. The actual optical path used in the experiments was 2.4 m, which was found from the concentrations of the reactants. Argon was filled into the cell to a pressure of 1.01×10^5 Pa at first and then evacuated to 20 Pa at ambient temperature before the sample placement. After the sample was placed, argon was filled into the cell again to 1.01×10^5 Pa, the spectrum of the background gases was measured, and then the cell was evacuated to 20 Pa again. Argon (purity >99.999%) was used as a carrier gas to load the reactive gases, SO_2 (0.2 mL, purity >99%) and O_2 (0.5 mL, purity >99.999%), into the cell through the six-way valves I and II, respectively. After the cell was filled to a pressure of 1.01×10^5 Pa, it remained at that pressure for 5 min to ensure homogeneous mixing of the gases in the cell before starting to measure the *in situ* IR spectra with a FTIR spectrometer (NICOLET Avatar 360) equipped with an MCT detector. Typically each spectrum was recorded by 250 scans on average at a resolution of 4 cm^{-1} over the range extending from 600 to 4000 cm^{-1}. A single-beam spectrum was used as a reference spectrum, which was taken prior to exposure of SO_2, to obtain the absorbance spectra of the gas phase. The quantification method of SO_2 was reliable with the linear correlation coefficient of 0.9998 for the standard curve. All the measurements were repeated at least twice.

***In Situ* DRIFTS Measurement.** The DRIFT technique was used to study the surface reactions. The powder of the sample was placed in the small chamber (inner diameter = 1 cm). Figure 2 shows the schematic diagram of the DRIFTS apparatus. Before the reaction gas was introduced, argon was flowed into (150 mL/min) the chamber to wash off water, physicsorbed impurities, and the powder on the surface of the chamber. Infrared spectra were recorded in the spectral range from 4000 to 400 cm^{-1} by using a Nicolet FTIR spectrometer, a Spectra-Tech Diffuse Reflectance Accessory, equipped with a MCT detector. Spectra were collected at a resolution of 4 cm^{-1} and a time resolution of 1 min when 100 scans on average were used for each spectrum. The losses of those species depleted in the surface reactions would show negative bands, and those of the products positive bands. It took 30 to 90 min to reach a stable condition when there was no apparent spectra variation, which indicated the formation of a clean surface of the powder for the reaction. A single-beam spectrum was used as a reference spectrum, which was collected prior to exposure of SO_2, to obtain the absorbance spectra of the gas phase. After collecting the background spectrum, SO_2 (0.6%) and O_2 (6.5%) were introduced to the chamber at the total flow rate of 156 mL/min.

Sources of Oxide Particles and Aerosol Sample Used in This Study. On the basis of comments on the oxides in the dust aerosol,[39] we choose the oxides Al_2O_3, CaO, TiO_2, MgO, FeOOH, Fe_2O_3, MnO_2, and SiO_2 as the typical mineral particles to be studied. All of those oxide particles except FeOOH used in these experiments were of AR (analytically pure) purity and were purchased commercially. FeOOH was prepared by titration of a 10% $FeCl_3$ solution with an ammonium hydroxide solution to a final pH of 8−9 under vigorously stirring conditions. The final solution was filtered and the precipitate was thoroughly washed with deionized water to remove the chlorine ions and dried at 60 °C for 6 h under a vacuum heating system. The atmospheric particle samples were collected at a flow rate of 77.59 L min^{-1} on the roof of a building on the Fudan University campus, Shanghai, using medium-volume pumps ((TSP/PM10/PM2.5)-2, DiKe Electronic Instrument Inc., Beijing, China). Nuclepore polycarbonate membrane filters (0.6 μm pore size, d = 90 mm) were used to collect the aerosol samples. The mixture used in this study was obtained by mixing the different oxides with the ratio that was calculated based on the abundance of those major elements in the continental crust[38] as SiO_2:Al_2O_3:Fe_2O_3:CaO:MgO:TiO_2:MnO_2 = 61.5:15.1:6.28:5.5:3.7:0.68:0.1.

Analytical Method. *XPS Analysis of the Aerosol Surface.* X-ray photoelectron spectroscopy (PHI 5000C, P. E. Inc. in the United States) was used for the surface analysis of the aerosol particle. The system used Al Kα as the irradiation source with the working power of 250 W at a voltage of 14.0 kV, and was calibrated against the C1s spectrum with Eb = 284.8 eV as the internal reference. The scanning range for acquiring spectroscopy is from 0 to 1200 eV. The minute spectroscopies of 10 elements (C1s, O1s, Na1s, Mg2p, Al2p, Si2p, S2p, Ca2p, Mn2p, Fe2p) were acquired. The special software PHI-MATLAB was used for data analysis.

Results and Discussion

***In Situ* FTIR Study of SO_2 Absorption on Mineral Oxides at Ambient Temperature.** Absorbance spectra of SO_2 on mineral oxides were obtained by referencing an oxide sample spectrum after SO_2 was introduced into the infrared cell to an

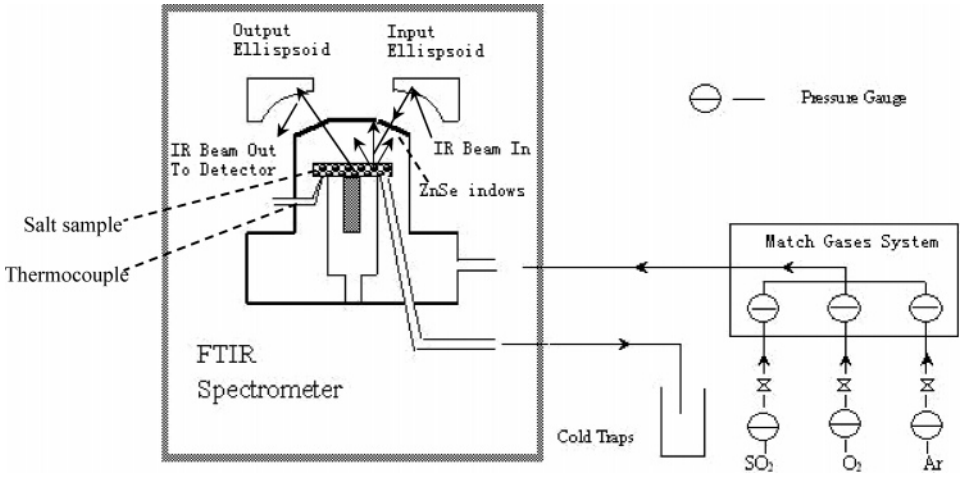

Figure 2. Schematic diagram of the DRIFT apparatus.

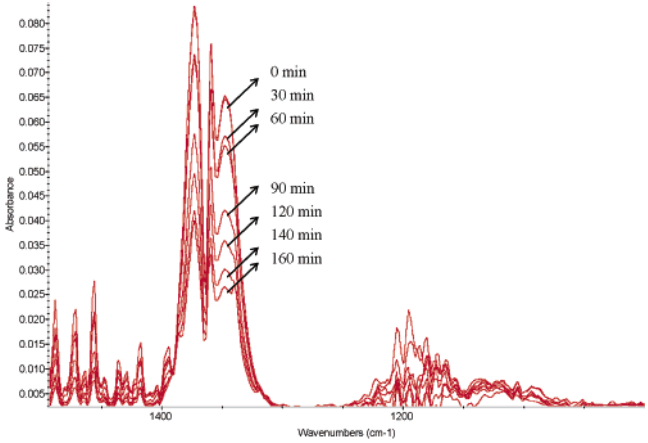

Figure 3. *In situ* FTIR spectra for the reaction of SO_2 with FeOOH.

oxide background spectrum prior to absorption. Changes in the infrared spectra of SO_2 are clearly seen in Figure 3. The strongest adsorption band between 1300 and 1400 cm^{-1}, with features at 1373, 1360, and 1348 cm^{-1}, was observed in the spectrum. Besides, there were some weak absorptions near 1550 and 1190 cm^{-1}, which were signed to the feature of H_2O produced from the reaction of SO_2 with surface hydroxyls. There were no other adsorption bands in the spectrum, which implied that there were no other gas products containing sulfur and the products were in the solid phase. The solid products were identified by surface analysis, XPS.

Comparison of the Reactivity of the Oxides. As SO_2 exposure decreased due to the absorption on oxides, the intensity of the prominent bands decreased in the spectra until the time when the surface of the oxides was saturated (Figure 4). It could be seen clearly that the reactivity varied with various oxides. The heterogeneous oxidation of SO_2 on the surface of FeOOH runs most rapidly at the initial stage. The conversion of SO_2 on FeOOH, Al_2O_3, and MgO in 2 h was up to 73%, 70%, and 58%, respectively. As to the reactivity of the mixture, the conversion of SO_2 was up to 57% in 2 h, which is much higher than the calculated value (24%) based on the composition−proportional contribution of each components (f-mixture $= \sum_i fi$). This result demonstrated that the components in the mixture apparently had a synergetic effect on the oxidation of SO_2. The conversion of SO_2 on the surfaces of TiO_2, Fe_2O_3, and SiO_2 in 2 h was 32%, 15%, and 14%, respectively. The reactivity of all these oxides with SO_2 was in the order of FeOOH > Al_2O_3 > mixture > MgO > TiO_2 > Fe_2O_3 > SiO_2.

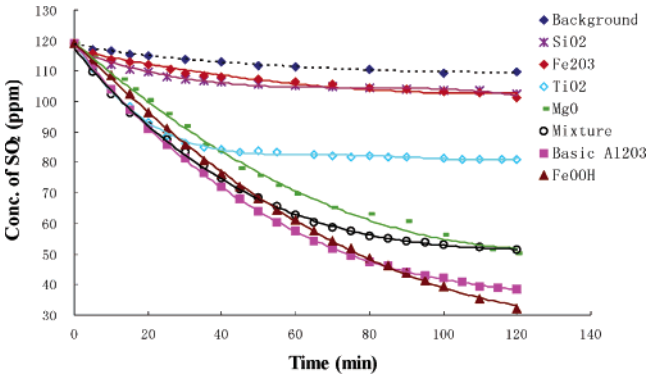

Figure 4. Time evolution of the concentration of SO_2 in the presence of different oxides.

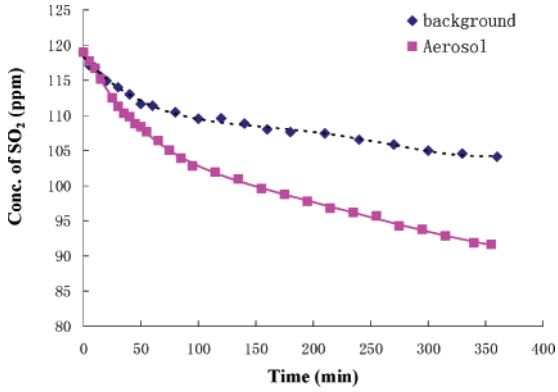

Figure 5. Time evolution of the concentration of SO_2 in the presence of field aerosol.

Field-collected aerosol was also investigated (Figure 5). The initial uptake of SO_2 on field aerosol in 2 h was determined to be 12%, which is higher than the background (8%), indicating the obvious conversion of SO_2 on the field-collected aerosols. The urban aerosols used in this study were the mixture of the mineral aerosol with pollution aerosol (sulfate, nitrate, and organic matters, etc.). By using the abundance (8%) of Al in the crust, the mineral aerosol could be calculated to be 34% of the total mass of the field-collected aerosol used in the experiment. The mineral aerosol was usually $\sim 1/3$ of the total mass concentration of the aerosol collected.[43,44] Also, in the field-collected aerosol part of mineral aerosol contained not only oxides but also aluminosilicate, which is less reactive compared with those oxides in the reaction with SO_2. Considering these factors mentioned above the 12% uptake of SO_2 on the field-

TABLE 1: Apparent Rate Constants and Half-Life of the Heterogeneous Reactions of SO_2 on Different Oxides

samples	apparent rate constant/s^{-1}	half-life/h	correlation coeff R^2
basic Al_2O_3	1.41×10^{-2}	0.855	0.9982
neutra Al_2O_3	1.35×10^{-2}	0.862	0.9967
acid Al_2O_3	1.26×10^{-2}	0.899	0.9903
TiO_2	1.12×10^{-2}	0.976	0.9961
$TiO\cdot nH_2O$	1.12×10^{-2}	1.031	0.9982
mixture	1.04×10^{-2}	1.049	0.994
FeOOH	1.03×10^{-2}	1.059	0.9966
MgO	9.0×10^{-3}	1.110	0.9967
SiO_2	3.1×10^{-3}	3.630	0.9069
Fe_2O_3	2.6×10^{-3}	4.380	0.9591

collected aerosol would be comparable to the 24% on the mixture sample.

The Kinetics of the Oxidation of SO_2 on the Surface of Oxides. Figure 4 showed the variations of the concentration of SO_2 while it reacted on the surface of different oxides: Al_2O_3, TiO_2, MgO, SiO_2, FeOOH, Fe_2O_3, and a mixture. In a closed White Cell with a total volume of 1.67 L the initial concentration of SO_2 that reacted with 30 mg of different oxides was 119 ppm. This heterogeneous reaction was most likely irreversible, as the reactants of SO_2 and O_2 were gases and one of the products was sulfate in the solid phase. The concentration of O_2 could be regarded as constant because it was very abundant as compared with SO_2. Judeikis et al.[26] reported that the heterogeneous oxidation of SO_2 on surfaces of the oxides was a pseudo-first-order reaction. The kinetics equation for the pseudo-first-order reaction should be as below:

$$-\mathrm{d}C_{SO_2}/\mathrm{d}t = K_{SO_2}C_{SO_{20}}$$

$$\ln[C_{SO_{20}}/C_{SO_2}] = K_{SO_2}t$$

where $C_{SO_{20}}$ was the initial concentration of SO_2. Table 1 shows that in the oxidation of SO_2 on the surface of most oxides the correlation coefficient of $\ln[C_{SO_{20}}/C_{SO_2}]$ vs time (t) was greater than 0.99. The results from this experiment indicated that these oxidations were pseudo-first-order reactions. However, the correlation coefficient of the oxidations of SO_2 on Fe_2O_3 and SiO_2 was less than 0.99 (Table 1), which could not be seen as a pseudo-first-order reaction fairly.

The apparent rate constants and the half-life of the oxidations of SO_2 with different oxides were shown in Table 1. The apparent rate constants were determined to be 1.35×10^{-2} and 9.4×10^{-3} for uptake on Al_2O_3 and MgO, respectively, which was in agreement with previous reports.[37, 39] The rate constant of the mixture of these oxides calculated from each individual component was 0.4×10^{-2} s^{-1}, which was lower than the experimental value of 1.0×10^{-2} s^{-1}, indicating that there could be a distinct synthetic effect of those individual components in the oxidation of SO_2 on the mixture.

The specific surface of each oxide was measured by the BET method, and the specific area catalytic activity of each oxide were exhibited in Table 2. The reactivity of all these oxides with SO_2 by specific area was in the order of Fe_2O_3 > MgO > TiO_2 > FeOOH > mixture > Al_2O_3 > SiO_2, completely different from the order with respect to mass. It could be seen clearly that the conversion rate of SO_2 per unit surface of Fe_2O_3 was the greatest among all the oxides, indicating that Fe_2O_3 could be the best one for the oxidation of SO_2 among all these oxides. Those dust particles containing iron might be effective in the reaction with SO_2. The earlier study with a simple method[24] reported a similar result to that we obtained in this study. Fe_2O_3 is one of the most important species in the process of exchange between atmosphere and oceans.[45, 46] The iron-containing compounds in the aerosols might play a complicated role in the conversion of sulfur species.[31,32]

TABLE 2. Conversion Rate of SO_2 per Unit Specific Surface Area on Different Oxides

oxides	BET/$m^2\cdot g^{-1}$	surface area/m^2	conversion rate of SO_2 in 2 h	reactivity order
Fe_2O_3	9.77	0.29	0.51	1
MgO	65.52	1.97	0.29	2
$TiO\cdot nH_2O$	82.05	2.46	0.29	3
TiO_2	48.40	1.45	0.22	4
FeOOH	118.07	3.54	0.21	5
mixture	105.28	3.16	0.18	6
basic Al_2O_3	146.30	4.39	0.16	7
neutral Al_2O_3	124.60	3.74	0.12	8
acid Al_2O_3	155.30	4.66	0.09	9
SiO_2	206.00	6.18	0.02	10

Effect of the Mass and the Apparent Surface Area of Oxides on the Oxidation of SO_2. In the early study,[26] the oxidation rate constant of SO_2 on oxide particles was reported to be independent of the thickness of the sample, which would indicate that only the very outer layer of the particles reacted with SO_2. However, there was no systematic study on the effect of the thickness of the oxide sample on the oxidation of SO_2 so far. Figure 6 showed the kinetics of the oxidation of SO_2 on the same area of the outer layer (1 pallet) of Al_2O_3 with different mass: one was 30 mg and the other 60 mg. It could be seen that although the initial oxidation rate was independent of the mass of the oxide, the final conversion of SO_2 in 2 h on the oxide of 60 mg was 76.9%, while on the oxide of 30 mg it was 67.8%. The result indicated that more mass of the same oxide could lead to more conversion of SO_2, although it was much less than the proportional value to the mass. Figure 7 showed the kinetics of the oxidation of SO_2 on the same mass (30 mg) of Al_2O_3 with different apparent area: 1 pallet of 2.66 cm^2 and 2 pallets of 5.32 cm^2. On the 1 pallet of Al_2O_3 the initial rate constant was 1.23×10^{-2} s^{-1}, while on 2 pallets it was 1.61×10^{-2} s^{-1}, which was faster than that with 1 pallet. The result indicated clearly that the greater the apparent area, the faster the conversion of SO_2. However, the conversions of SO_2 in 2 h in the two cases were similar: 67.8% for 1 pallet and 66.5% for 2 pallets.

The Products of the Oxidation of SO_2 on the Surface of Oxides Detected by DRIFTS. Diffuse Reflectance Infrared Fourier Transform Spectroscopy (DRIFTS) was used to investigate the nature of the surface-bound species formed with the uptake of gas-phase SO_2 on the oxide particles. Figures 8 and 9 showed the representative spectra of the products of the oxidation of SO_2 on the surface of Al_2O_3 and MgO. Similar spectra were observed for most of the oxides, except for MnO_2 and SiO_2, in which there were no obvious absorption bands. Upon exposure of SO_2, new absorptions in the spectral range were evidently observed in the spectra of those oxides. As SO_2 exposure increased, the intensity of the prominent bands in the spectra increased until the time for the surface of the oxides to be saturated. Figures 8 and 9 showed the representative spectra of the products of the oxidation of SO_2 on the surface of Al_2O_3 and MgO. The absorption bands between 800 and 1300 cm^{-1} could be assigned with the aid of the previous infrared studies of SO_2 absorption on surfaces of these oxides.[27,28,37,38,47−51] Those spectra indicated clearly the changes in the hydroxyl region upon adsorption of SO_2. The growth of a broad band between 3300 and 3650 cm^{-1} could be seen, which was upon the evacuation of the gas phase. The negative features of the

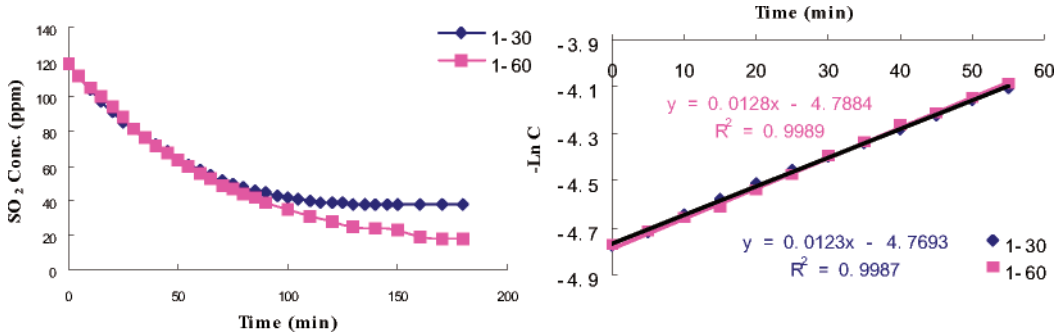

Figure 6. Kinetics of SO_2 reaction on Al_2O_3 of different mass with the same apparent area: **1**−**30**, 1 pallet of Al_2O_3, 30 mg; **1**−**60**, 1 pallet of Al_2O_3, 60 mg.

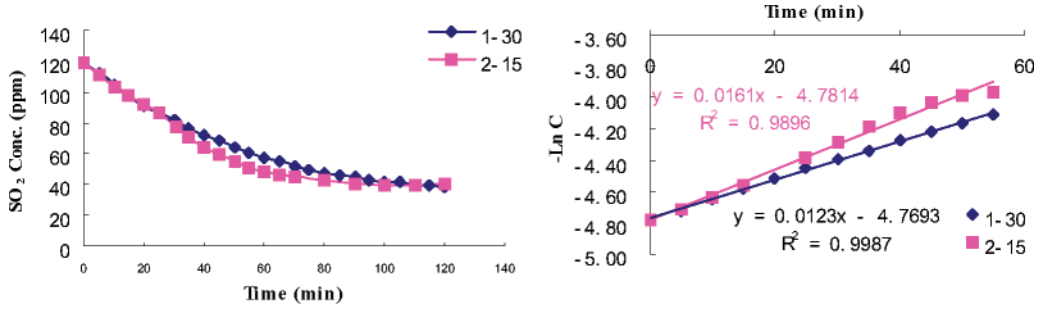

Figure 7. Kinetics of SO_2 reaction on Al_2O_3 of the same mass with different apparent area: **1**−**30**, 1 pallet of Al_2O_3, 30 mg; **2**−**15**, 2 pallets of Al_2O_3, 15 mg per pallet.

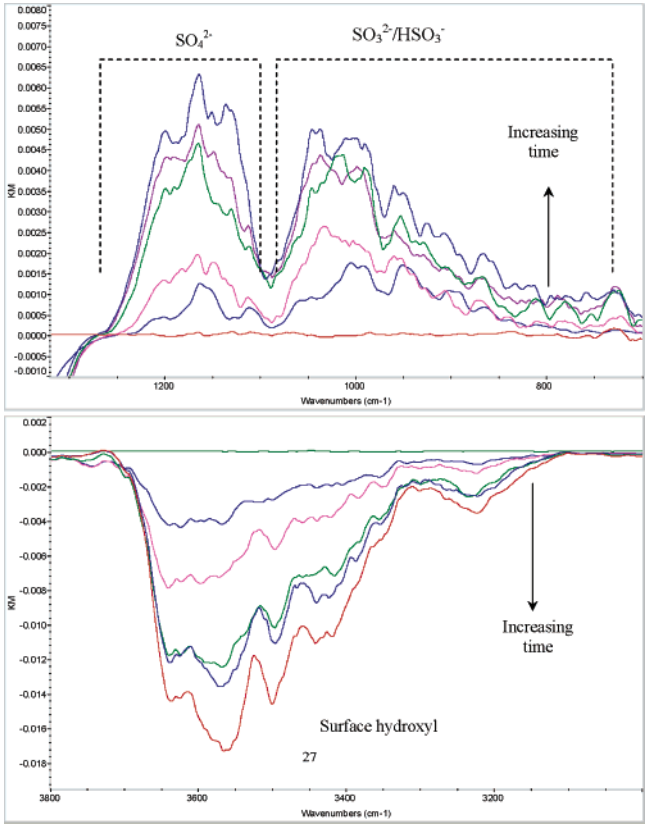

Figure 8. DRIFTS spectra of different species produced on Al_2O_3 following exposure to gas-phase SO_2.

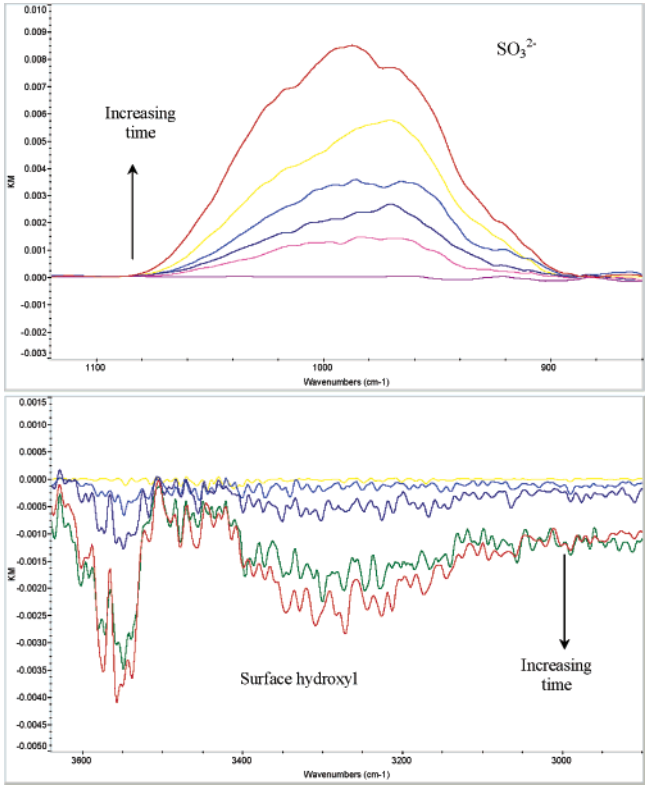

Figure 9. DRIFTS spectra of different species produced on MgO following exposure to gas-phase SO_2.

spectra indicated either loss from the surface or being involved in hydrogen bonding of the hydroxyl groups. The spectra of the oxides investigated exhibited similar features to those in the literature. The bands from 850 to1100 cm^{-1} could be assigned to the stretching motion of adsorbed sulfite, SO_3^{2-}, and/or bisulfite, HSO_3^-. The stretching motion of adsorbed sulfate, SO_4^{2-}, contributed to the bands between 1100 and 1300 cm^{-1}. There could be several types of coordination environments or coordinates (monodentate and bidentate) to the surface, as the breadth of bands and the number of bands with a wider range of breadth were observed in the region from 850 to 1300 cm^{-1}.

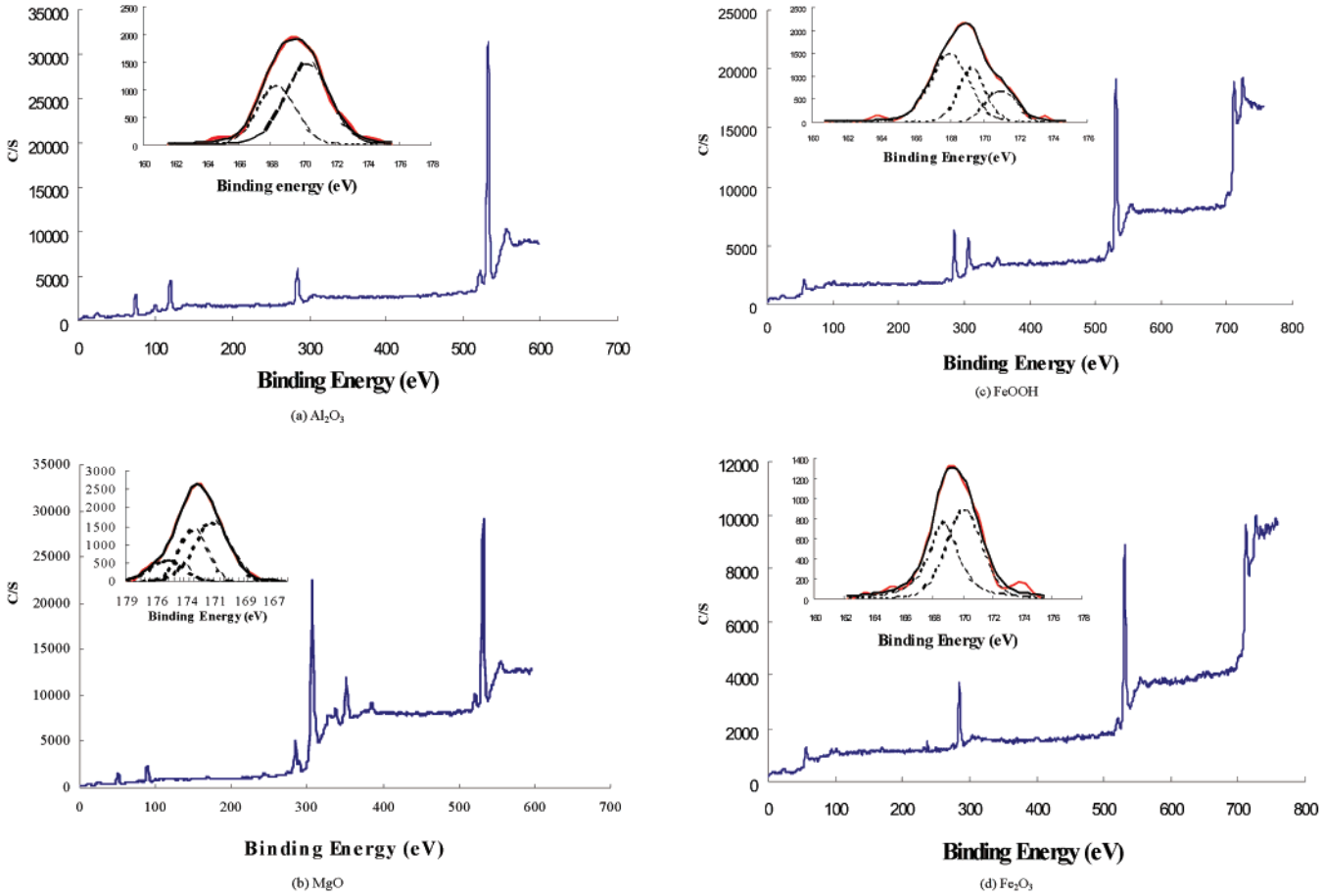

Figure 10. XPS spectra of various species produced on the surface of the different oxides: (a) Al_2O_3, (b) MgO, (c) FeOOH, and (d) Fe_2O_3.

Changes in the infrared spectra on the surface of Al_2O_3 with the increase of SO_2 were clearly seen in Figure 8. Upon adsorption of SO_2 on Al_2O_3 particles, a broad absorption band between 800 and 1300 cm^{-1} was observed. The intensity of this broad band grew as SO_2 exposure increased until the time when the surface was saturated. The strong broad absorption band in the spectra between 800 and 1300 cm^{-1} remained when a blow-off process with argon was carried out. This indicated that the surface adsorbed species with the broad absorbance bands between 800 and 1300 cm^{-1} was chemisorbed on the Al_2O_3 particles and could not be removed by the blow-off process with argon. The broad absorption band between 800 and 1100 cm^{-1} in the Al_2O_3 spectrum was composed of more than one band and could be assigned to the absorptions of sulfite and bisulfite on the surface, while SO_4^{2-} contributed to several bands in the absorption band range between 1100 and 1300 cm^{-1}. The assignment of these vibrational bands of adsorbed sulfur dioxide was discussed previously.[49−51] The infrared spectra obtained from the adsorption of SO_2 on Al_2O_3 in this study agreed well with other infrared studies reported in the literature. Mitchell et al.[51] and Chang[48] investigated SO_2 adsorption on Al_2O_3 particles with infrared spectroscopy and found that the broad band between 800 and 1100 cm^{-1} was assigned to the strongly adsorbed SO_2, which was identified as a sulfite species. For the highly hydroxylated alumina surfaces, such as the ones used in this study, the product on the surface could be identified as sulfate as well. The surface hydroxyls and lattice oxygen atoms could react with SO_2 to form sulfite and sulfate (see the detailed discussion in the section on the reaction mechanism below).

Figure 9 showed clearly the changes in the infrared spectra on the MgO surface with the increase of SO_2 exposure. A strongly adsorbed species was formed following the exposure of MgO to gaseous SO_2, which showed a strong broad absorption range between 880 and 1100 cm^{-1} with several bands. These bands remained in the spectrum upon evacuation of SO_2 vapor, and they could be assigned to surface-coordinated sulfite. This interpretation was in agreement with the early studies of SO_2 adsorption on the basic oxides, MgO and CaO.[27] Goodsel et al.[28] listed the bands at 1041 and 956 cm^{-1} as belonging to a monodentate surface sulfitocomplex (n3 and n1 modes and bands at 1062 and 954 cm^{-1} that corresponded to a bidentate surface sulfitocomplex). DRIFTS could provide further evidence that SO_2 reacts with mineral particles to produce surface-coordinate sulfite and sulfate on the surface of the oxides.

The Products of the Oxidation of SO_2 on the Surface of Oxides Detected by XPS Analysis. Figure 10a−d exhibited XPS spectra that were used to determine the chemical speciation of the products of the oxidation of SO_2 on the surface of Al_2O_3, MgO, FeOOH, and Fe_2O_3, respectively, and their corresponding simulant peaks of sulfur. In Figure 11a, the observed peaks at the binding energy of 74.35, 119.35, and 535.80 eV were signals of Al_{2p}, Al_{2s}, and O_{1s}, respectively, which were attributed to Al_2O_3 itself. There was one new adsorption peak (see the enlarged one) that could be the combination of two peaks at the binding energy of 168.34 and 170.25 eV. The peak at the binding energy of 168.34 eV could be the adsorption peak of S_{2p} of SO_3^{2-}, and the latter one of 170.25 eV could be the adsorption peak of S_{2p} of SO_4^{2-}. The observed spectrum peaks

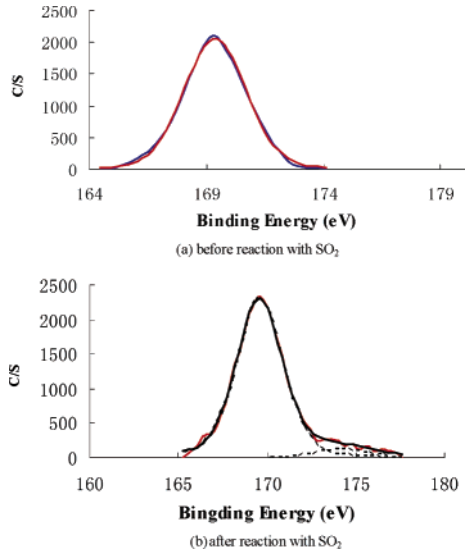

Figure 11. XPS spectra of S species on the filed aerosol before and after reaction with SO_2: (a) before reaction with SO_2 and (b) after reaction with SO_2.

in Figure 11b were at the binding energy of 88.2, 287.15, and 536.30 eV, which were signals of Mg_{2s}, C_{1s}, and O_{1s}, respectively, and they were attributed to MgO itself. An S peak was observed that could be the combination of three peaks at the binding energy of 167.9, 169.5, and 171.5 eV, which corresponded to the adsorption of S_{2p} of SO_2, SO_3^{2-}, and an unknown species that was not listed in the handbook of X-ray Photoelectron Spectroscopy.[52] Figure 11c exhibited the observed peaks at the binding energy of 724.68, 714.18, 287.15, and 536.30 eV, which were signals of $Fe_{2p1/2}$, $Fe_{2p3/2}$, C_{1s}, and O_{1s}, respectively, and they were attributed to FeOOH itself. An S peak was also observed, and it could be the combination of three peaks at the binding energy of 167.96, 169.16, and 170.96 eV, which corresponded to the adsorption of S_{2p} of $FeSO_4$, $Fe_2(SO_4)_3$, and SO_3^{2-}. The relative concentration ratio of $[SO_3^{2-}]$ to $[SO_4^{2-}]$, which was calculated from the peak area of the corresponding species on the XPS spectra, was 18:82, indicating that 82% of the total gas-phase SO_2 adsorbed on the surface of FeOOH was converted to sulfate, SO_4^{2-}, and the rest of 18% of S(IV) was not converted to S(VI), instead, they exited in the form of the species SO_3^{2-}. Figure 10d showed the peaks of $Fe_{2p1/2}$ (724.49 eV), $Fe_{2p3/2}$ (714.18 eV), O_{1s} (536.30 eV), and C_{1s} (286.61 eV), which were all attributed to Fe_2O_3 itself. The S peak observed on the surface of Fe_2O_3 was the combination of the two peaks at the binding energy of 168.67 and 170.06 eV, which could be the S_{2p} of $SO_4^{2-}$and SO_3^{2-}. The relative concentration ratio of $[SO_3^{2-}]$ to $[SO_4^{2-}]$ was 53:47. It could be seen clearly that on the surface of FeOOH the converted fraction of the absorbed SO_2 from S(IV) to S(VI) was 82%, much higher than that of 47% on Fe_2O_3, which demonstrated that the surface structure and the composition of FeOOH was more favorable than $Fe_2O_3$for the conversion of SO_2 to be SO_4^{2-}.

Figure 11 showed the XPS spectra of the various sulfur species on the field-collected aerosol before and after reaction with SO_2. The speciation of S on the aerosol surface was in the form of SO_4^{2-}, which accounted for 2.6% of the total surface concentrations of the 10 elements (S, C, O, Si, Fe, Ca, Mg, Mn, Na, and Al) measured. After reaction with SO_2 the speciation of S on the aerosol surface was in the form of both SO_3^{2-} and SO_4^{2-} with the relative concentration ratio of $[SO_3^{2-}]$ to $[SO_4^{2-}]$ of 7:93, and the sum of both S species on the aerosol

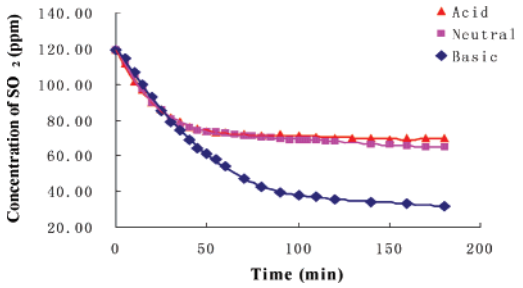

Figure 12. Time evolution of the concentration of SO_2 in the presence of Al_2O_3 with different acidity.

surface accounted for 3.5% of the total surface concentration. It could be seen clearly that when SO_2 went through the field-collected aerosol it could be adsorbed and reacted with the components on the surface of the aerosol and then most (93%) of them could be converted to sulfate, i.e., SO_4^{2-}, via the heterogeneous reaction with all kinds of mineral components on the surface of the aerosol, as it could be seen that the SO_4^{2-} species contributed to the total surface concentration of the 10 elements measured increased from 2.6% to 3.26% after reaction with SO_2.

The Mechanism of the Heterogeneous Reactions of SO_2 on Al_2O_3 Oxides. Under room temperature the gas-phase SO_2 could not react with O_2 in the air directly, whereas it could react with O_2 on the surface of those oxides, such as Al_2O_3 and Fe_2O_3, and form the products HSO_3^-, SO_3^{2-}, and SO_4^{2-} on the surface of the solid phase, as discussed in the above sections. Goodman et al.[37] and Usher et al.[38] reported that it could form HSO_3^- and SO_3^{2-} on the surface of the Al_2O_3 particle through the heterogeneous reaction with SO_2. It could be seen that the heterogeneous reaction of SO_2 with the mineral particles was one of the important pathways to increase the amount of sulfate coated on the aerosol particles.

Hydroxyls on the surface of the oxides are essential for this heterogeneous reaction. Basic, neutral, and acidic Al_2O_3 were investigated to compare their performance for the heterogeneous oxidation of SO_2. As shown in Figure 12, the concentrations of SO_2, which reacted with the three different kinds of Al_2O_3, i.e., basic, neutral, and acid, decrease rapidly at the initial stage of the reaction, and slow with the elapse of the reaction time in all the three cases. After the first 30 min in the cases of acidic and neutral Al_2O_3, the decrease of SO_2 concentration was very slow, while in the case of basic Al_2O_3, the decrease of SO_2 concentration did not slow until 100 min had passed. As shown in Table 1, the apparent rate constants of the oxidation of SO_2 on the different kinds of Al_2O_3 were in the order of basic γ-Al_2O_3 > neutral η-Al_2O_3 > acidic γ-Al_2O_3. The different acidity of the different kinds of Al_2O_3 was due to the different amounts of hydroxyls on the surface of them. Basic Al_2O_3 contains much more $Al(OH)_3$, i.e., more hydroxyls, than the acidic and neutral, implying that more hydroxyls on the surface of Al_2O_3 could be more in favor of the heterogeneous oxidation of SO_2.

Gasses, such as O_2 and H_2O(g), are prone to be adsorbed on the surface of oxides and form the active oxygen and hydroxyl on the surface. As mentioned above, SO_2 reacted with Al_2O_3 particles and produced a larger fraction of the strongly adsorbed and surface-coordinated sulfite/bisulfite, and sulfate on the surface. Thus a mechanism could be postulated for the reaction of SO_2 on Al_2O_3 particles as below: at first SO_2 could be weakly adsorbed on the surface of the acidic Al_2O_3 particles, while SO_2 could interact with the basic anions or hydroxides on the surface of the basic Al_2O_3 particle, and formed the surface-coordinated

sulfite. The early study[53] elaborated that adsorption of SO_2 on Lewis acid sites (coordinately unsaturated aluminum atoms) resulted in weakly adsorbed SO_2. Adsorption of SO_2 on Lewis base sites (exposed oxygen atoms) followed by rearrangement where the sulfite species attaches to aluminum through the sulfur atom resulted in chemisorbed sulfite. The surfaces of various Al_2O_3 particles could be covered with hydroxyl groups that were most likely involved in the production of both SO_3^{2-}/HSO_3^- and SO_4^{2-} on the surface while interacting with SO_2. Several heterogeneous reactions are proposed below for the production of surface-coordinated sulfite, bisulfite, and sulfate on the surface of the hydroxylated Al_2O_3 particle:

$$[O^{2-}]-M + SO_2(g) \rightarrow [SO_3^{2-}]-M(s) \quad (1)$$

$$[OH^-]-M + SO_2(g) \rightarrow [HSO_3^-]-M(s) \quad (2)$$

$$2[OH^-]-M + SO_2(g) \rightarrow [SO_3^{2-}]-M(s) + H_2O \quad (3)$$

$$2[SO_3^{2-}]-M(s) + O_2(g) \rightarrow 2[SO_4^{2-}]-M \quad (4)$$

$$2[HSO_3^-]-M(s) + O_2(g) + 2[OH^-]-M \rightarrow 2[SO_4^{2-}]-M + 2H_2O \quad (5)$$

where O^{2-} is lattice oxygen atom and OH^- is the adsorbed hydroxyl. As shown above, the surface hydroxyls on the surface of Al_2O_3 were in favor of the conversion of SO_2 to SO_3^{2-}/SO_4^{2-}, which was confirmed by the fact that the reactivity of basic Al_2O_3 was much greater than that of the acidic and neutral Al_2O_3.

The surface reaction of SO_2 with MgO appeared to follow somewhat a different mechanism, as on the surface of MgO there might be no as many hydroxylated species as on the surface of Al_2O_3. XPS data showed that on the surface of MgO particles there is strongly adsorbed surface-coordinated sulfite while SO_2 reacted with it. The formation of the surface-coordinated sulfite could be due to the interaction of the sulfur atom in SO_2 with four-coordinated O^{2-} anions. Pacchioni et al.[54] conducted a theoretical study of the adsorption and reaction of SO_2 on clean, completely dehydroxylated MgO surfaces. It was suggested that sulfite could form by interaction of the sulfur atom in SO_2 with two surface five-coordinated O^{2-} anions, i.e., two oxide anions on the unreconstructed MgO surface. It was predicted that the MgO surface would be especially suited for $MgSO_3$ formation because the separation between the two lattice oxygens of MgO was 0.297 nm, which was near the spacing of oxygens in bulk SO_3^{2-} powders, 0.270 nm. However, this structure was found to be highly repulsive and SO_2 dissociates spontaneously because the five-coordinated oxide anions did not offer enough basic character. The four-coordinated oxide anions, which were commonly found on steps and corners of MgO, have more basic character. These anions might provide favorable sites for sulfite formation. The MgO particles used in this study were powders, not single crystals, and the MgO particles could be expected to have more defects, steps, and kinks (more four-coordinated oxide anions) available for the reaction and might stabilize the formation of sulfite on MgO particles at room temperature. This could be the reason we observed a quantity of SO_3^{2-} on MgO particles.

The variety of reactivity of the different oxides with SO_2 is related to their intrinsic properties. For those metal oxides that have empty or half-empty d atom orbits, such as Al_2O_3, they are apt to adsorb O_2 and $H_2O(g)$ and form the surface hydroxyls and show an excellent performance in the reaction with SO_2, while for those metal oxides that have full d atom orbits, such as MnO_2, they show a weak reactivity in the heterogeneous reaction with SO_2.

Conclusions

(1) SO_3^{2-}, HSO_3^-, and SO_4^{2-} were formed on mineral particles as the products of the heterogeneous reaction of SO_2 on the surface of oxides and mineral aerosols. Surface-active oxygen and hydroxyl on the mineral particles were the key factors to the conversion of SO_2 to SO_3^{2-}, HSO_3^-, and SO_4^{2-}.

(2) The reactivity of the oxides with SO_2 was variable because of the different surface properties. FeOOH showed the best reactivity in the heterogeneous reactions of these oxides with the same mass; however, on the bases of the same surface area Fe_2O_3 could be most reactive in the reaction with SO_2 compared with all other particles. The mixture of these oxides exhibited a much higher conversion rate of SO_2 than the theoretic value (24%) based on the contribution of each individual component, indicating that the components in the mixture were not mixing simply and they had a synergetic effect on the oxidation of SO_2.

(3) The greater the apparent surface area of the oxides, the faster the oxidation of SO_2. The greater mass could also result in greater conversion of SO_2 on the surface of the oxides.

(4) The oxidations of SO_2 on the surface of most oxides were a pseudo-first-order reaction with respect to SO_2.

(5) The apparent rate constants were determined to be 1.35×10^{-2} and 9.4×10^{-3} for uptake on Al_2O_3 and MgO, respectively, which are similar to the results other scientists.

Acknowledgment. This work was supported by the National Natural Science Foundation of China (Grant Nos. 30230310, 20077004, and 20477004), Beijing Natural Science Foundation (Grant Nos. 8991002 and 8041003), and also in part by SKLLQG, the Institute of Earth Environment, CAS and LAPC, the Institute of Atmospheric Physics, CAS, the Swedish International Development Cooperation Agency (SIDA) through the Asian Regional Research Program on Environmental Technology (ARRPET) at the Asian Institute of Technology, and the National Basic Research Program of China (No. 2005CB422200x).

References and Notes

(1) Song, C. H.; Carmichael, G. R., *Atmos. Environ.* **1999**, *33*, 2203−2218.

(2) Kerminen, V.; Pirjola, L.; Boy, M.; Eskola, A.; Teinila, K.; Laakso, L.; Asmi, A.; Hienola, J.; Lauri, A.; Vainio, V.; Lehtinen, K.; Kulmala, M. *Atmos. Res.* **2000**, *54*, 41−57.

(3) Hegg, D. A.; Majeed, R.; Yuen, P. F.; Baker, M. B.; Larson, T. V. *Geophys. Res. Lett.* **1996**, *23*, 2613−2616.

(4) Han, J. H.; Martin, S. T. *J. Geophys. Res.-Atmos.* **1999**, *104*, 3543−3553.

(5) Martin, S. T. *Chem. Rev.* **2000**, *100*, 3403−3453.

(6) Dentener, F. J.; Carmichael, G. R.; Zhang, Y.; Leieveld, J.; Crutzen, P. J. *J. Geophys. Res*. **1996**, *101*, 22869−22888.

(7) Levin, Z.; Ganor, E.; Gladstein, V. *J. Appl. Meteorol.* **1996**, *35*, 1511−152.

(8) Luria, M.; Sievering, H. *Atmos. Environ*. **1991**, *25A*, 1489−1496.

(9) Song, C. H.; Phadnis, M.; Carmichael, G. R.; Underwood, G. M.; Miller, T. M.; Balster, E. T.; Grassian, V. H. Modeling Heterogeneous Reactions in Air Pollution Models. In *Air Pollution VII*; WIT Press: Boston, MA, 1999,; pp 685−695.

(10) Roth, B.; Okada, K. *Atmos. Environ*. **1998**, *32*, 1555−1569.

(11) Choi, J. C.; Lee, M.; Chun, Y.; Kim, J.; Oh, S. *J. Geophys. Res.* **2001**, *106*, d16, 18067−18074.

(12) Kim, B.; Park, S. *Atmos. Environ*. **2001**, *35*, 3191−3201.

(13) Fang, M.; Zheng, M.; Wang, F.; Chim, K. S.; Kot, S. C. *Atmos. Environ*. **1999**, *33*, 1803−1817.

(14) Zhuang, H.; Chan, C. K.; Fing, M.; Wexler, A. S. *Atmos. Environ*. **1999**, *33*, 4223−4233.

(15) Fan, X.; Okada, K.; Nimura, N.; Kai, K.; Arao, K.; Shi, G. Y.; Qin, Y.; Mitsuta, Y. *Atmos. Environ.* **1996**, *30*, 347−351.
(16) Ma, C. J.; Kasahara, M.; Holler, R.; Kamiya, T. *Atmos. Environ.* **2001**, *35*, 2707−2714.
(17) Jayne, J. T.; Davidovits, P.; Worsnop, D. R.; Zahniser, M. S.; Kolb, C. E. J. *J. Phys. Chem.* **1990**, *94*, 6041−6052.
(18) Martin, L. R.; Good, T. W. *Atmos. Environ.* **1991**, *25A*, 2395−2399.
(19) Sievering, H.; Boatman, J.; Galloway, J.; Keene, W.; Kim, Y.; Luria, M. *Atmos. Environ.* **1991**, *25A*, 1479−1487.
(20) Keene, W. C.; Sander, R.; Pszenny, A. A. P. *J. Aerosol Sci.* **1998**, *29*, 339−356.
(21) Capaldo, K.; Corbett, J. J.; Kasibhatla, P.; Fischbeck, P.; Pandis, S. N. *Nature* **1999**, *400*, 743−746.
(22) Krischke, U.; Staubes, R.; Brauers, T.; Gautrois, M.; Burkert, J.; Stobener, D.; Jaeschke, W. *J. Geophys. Res.* **2000**, *105*, 14412−14422.
(23) Maahs, H. G. *Atmos. Environ.* **1983**, *17*, 341−345.
(24) Urone, P.; Lutsep, H.; Noyes, C. M.; Parcher, J. F. *Environ. Sci. Technol.* **1968**, *2*, 611−618.
(25) Smith, B. M.; Wagman, J.; Fish, B. R. *Environ. Sci. Technol.* **1969**, *3*, 558−562.
(26) Judeikis, H. S.; Wren, A. G. *Atmos. Environ.* **1978**, *12*, 2315−2322.
(27) Low, M. J. D.; Goodsel, A. J.; Takezawa, N. *Environ. Sci. Technol.* **1997**, *5*, 1191−1195.
(28) Goodsel, A. J.; Low, M. J. D.; Takezawa, N. *Environ. Sci. Technol.* **1972**, *6*, 268−273.
(29) Arias, A. M.; Garcia, M. F.; Juez, A. I. *Appl. Catal. B* **2000**, *28*, 29−41.
(30) Mochida, M.; Pitts, *J. Phys. Chem. A* **2000**, *104*, 9705−9711.
(31) Wang, L.; Zhang, F.; Chen, J. M. *Sci. China, Ser. B: Chem., Life Sci., Earth Sci.* **2001**, *44* (6), 587−595.
(32) Wang, L.; Zhang, F.; Chen, J. M. *Environ. Sci. Technol.* **2001**, *35* (12), 2543−2547.
(33) Wang, L.; Song, G. X.; Zhang, F. *Gaodeng Xuexiao Huaxue Xuebao* **2002**, *23* (9), 1738−1742.
(34) Wu, H.; Wang, X.; Chen, J. *Chin. Sci. Bull.* **2004**, *49* (12), 1231−1235.
(35) Wu, H.; Wang, X.; Chen, J. *Sci. Chin. Ser. B: Chem.* **2005**, **48** (1), 31−37.
(36) Carlos-Cuellar, S.; Li, P.; Christensen, A. P.; Krueger, B. J.; Burrichter, C.; Grassian, V. H. *J. Phys. Chem. A* **2003**, *107*, 4250−4261.
(37) Goodman, A. L.; Li, P.; Usher, C. R.; Grassian, V. H. *J. Phys. Chem. A* **2001**, *105*, 6109−6120.
(38) Usher, C. R.; Al-Hosney, H.; Carlos-Cuellar, S.; Grassian, V. H. *J. Geophys. Res.* **2002**, *107* (D23), ACH16-1−ACH16−9.
(39) Courtney, R.; Usher, C.; Michel, E.; Vicki, H. Grassian, V. H. *Chem. Rev.* **2003**, *103*, 4883−4939.
(40) Meskhidze, N.; Chameides, A. L.; Nenes, A.; Chen, G. *Geophys. Res. Lett.* **2003**, *30* (21), ASC 2−1∼2−5.
(41) Zhang, X.; Zhuang, G.; Chen, J.; Xue, H. *Chin. Sci. Bull.* **2005**, *50* (8), 738−744.
(42) Jickells, T. D.; An, Z. S.; Andersen, K. K.; Baker, A. R.; Bergametti, G.; Brooks, N.; Cao, J. J.; Boyd, P. W.; Duce, R. A.; Hunter, K. A.; Kawahata, H.; Kubilay, N.; laRoche, J.; Liss, P. S.; Mahowald, N.; Prospero, J. M.; Ridgwell,A. J.; Tegen, I.; Torres, R. *Science* **2005**, *308*, 67−71.
(43) Sun, Y.; Zhuang, G.; Yuan, H.; Zhang, X.; Guo, J. *Chin. Sci. Bull.* **2004**, *49* (7), 698−705.
(44) Han, L.; Zhuang, G.; Sun, Y.; Wang, Z. *Chin. Sci. B: Chem.* **2005**, *48* (4), 253−264.
(45) Zhuang, G.; Yi, Z.; Duce, R. A. *Nature* **1992**, *355*, 537−539.
(46) Zhuang, G.; Guo, J.; Yuan, H. *Chin. Sci. Bull.* **2003**, *48* (11), 1080−1086.
(47) Deo, A. V.; Dalla Lana; I. G.; Habgood, H. W. *J. Catal.* **1971**, *21*, 270−281.
(48) Chang, C. C. *J. Catal.* **1978**, *53*, 374−385.
(49) Lavalley, J. C.; Janin, A.; Kinet, J. *Catal. Lett* **1981**, *18*, 85−88.
(50) Datta, A.; Cavell, R. G.; Tower, R. W.; George, Z. M. *J. Phys. Chem.* **1985**, *89*, 443−449.
(51) Mitchell, M. B.; Sheinkar, V. N.; White, M. G. *J. Phys. Chem.* **1996**, *100*, 7550−7557.
(52) Wagner, C. D.; Riggs, W. M.; Davis, L. E. *Handbook of X-ray Photoelectron Spectroscopy*; Chastain, J., Ed.; Perkin-Elmer Corporation, Physical Electronics Division: Eden Prairie, MN, 1992.
(53) James, W.; William, F. B. *Thermochim. Acta* **1996**, *288*, 179−189.
(54) Pacchioni, G.; Clotet, A.; Ricart, J. M. *Surf. Sci.* **1994**, *315*, 337−350.